Large Energy Q-Switched Fiber Laser With Black Phosphorus Saturable Absorber Fabricated by Sol−Gel Technique

Zhendong Chen , Tianyu Liu , Duo Pan , Yonggang Wang , Yajun Li , and Jianjun Wu

Abstract—**Black phosphorus (BP) has attracted extensive attention due to its unique optical and electrical properties. However, BP is easily oxidized in the air, which significantly limits its application. In this study, BP is successful doped into sol-gel glass, it shows excellent chemical stability in atmospheric environment for five months. In addition, as a kind of inorganic matrix, optical damage threshold of BP-doped sol-gel glass reaches as high as 51.69 GW/cm^2, which is six times higher than that of plastic polymer. Saturable absorption parameters of the BP are maintained after five months in the air. The BP-doped sol-gel glass is inserted into erbium-doped fiber (EDF) laser to realize passively Q-switched and mode locked operation. Compared to most Q-switched EDF lasers based on broadband absorbers, the single pulse energy is one of the highest values (315.99 nJ). Overall, these data evidently provide a practical solution to stabilize BP in the air by embedding it in the silica, and also open the way for extensive applications of BP.**

Index Terms—**Black phosphorus, sol−gel technique, erbium-doped fiber, saturable absorber.**

I. Introduction

BLACK phosphorus (BP), a graphene analogue two-dimensional (2D) material, has attracted tremendous interest due to its exceptional properties, including tunable electronic band gap, large on/off ratios, fast response time, and high carrier mobility [1], [2], [3], [4]. Especially, BP has great application prospects as saturable absorber (SA) [5], [6]. Differing from graphene, BP's band gap can vary with the number of layers (from 0.3 eV to 2.0 eV) [7], [8], [9], [10], [11], filling up the gap between the graphene (zero-band gap) and the transition metal dichalcogenides (the wide band gap) [12], [13], [14]. Therefore, BP is a universal SA covering illumination of visible to mid-infrared bands [15], [16].

Unfortunately, BP cannot be directly used in the atmosphere due to its instability, which impedes practical applications.

Zhendong Chen, Tianyu Liu, Duo Pan, and Jianjun Wu are with the School of Electronics, Peking University, Beijing 100871, China (e-mail: panduo@pku.edu.cn).

Yonggang Wang is with the School of Physics and Information Technology, Shaanxi Normal University, Xi'an 710119, China (e-mail: chinawygxjw@snnu.edu.cn).

Yajun Li is with the Engineering Research Center of Integrated Circuit Packaging and Testing, Ministry of Education, Tianshui Normal University, Tianshui 741099, China.

covalent grafting and non-covalent coatings have been developed to avoid oxidation and degradation of BP [17], [18]. However, the surface chemical bonds of BP will be changed in the process of covalent grafting, which inevitably affects its properties. Therefore, it is necessary to develop non-covalent passivation. Many polymers have successfully been used to protect BP such as like polyvinyl alcohol (PVA), polymethyl-methacrylate (PMMA), and polycarbonate [19], [20], [21], [22], [23], [24], [25], [26]. Although polymer composite films are optically transparent in the spectrum range of interest, they have very low optical damage thresholds and mechanical stability, which limit their application in high power and long time laser [19], [20], [21], [22], [23], [24], [25], [26].

Thus, it is imperative for BP to be dispersed into the inorganic material with high damage threshold and high transmission. However, the inorganic material is usually prepared at very high temperature, such as manufacturing process of optical fibers, in which BP will be oxidized. Accordingly, we propose to encapsulate BP into glass at room temperatures using sol-gel technology, the sol-gel glass is compact and smooth during preparation by using the acidic as catalyst, so it can effectively encapsulate BP [27], [28], [29], [30]. In addition, the main component of sol gel glass is silicon dioxide, it has characteristics similar to ordinary fiber, such as refractive index, laser absorption, mechanical strength, and thermal properties. Therefore, it is very advantageous to apply BP-doped sol-gel glass to fiber lasers.

In this work, a novel technology is employed to prevent the oxidation of BP. The BP doped in sol-gel glass not only is air-stable, but also can withstand large energy laser. By inserting BP-doped sol-gel glass into the EDF laser cavity, both Q-switched and mode locking operation are obtained. Benefited from high optical damage threshold of SA, this Q-switching fiber laser works in a broader pump range (from 93 mW to 610 mW). The pulse width decreases from 7.83 μs to 1.53 μs and the single-pulse laser energy increases from 92.41 nJ to 315.99 nJ with the increasing of the pump power. Our works provide a practical solution to stabilize BP in the air and enable the development of BP-based materials for nonlinear applications.

II. Materials, Methods and Characterizations

A. Preparation of BP-Doped Sol-Gel Glass

The preparation process is shown in Fig. 1. Firstly, the BP solution is prepared using physical ultrasonic agitation: 10-mg BP
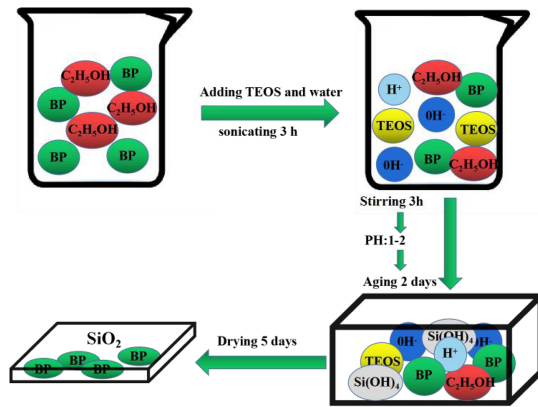
Fig. 1.   Preparation procedure of BP-doped sol-gel glass. Water and TEOS ($C_8O_4H_{20}Si$ A.R.) are used as reactants in the experiment. Because water and TEOS are incompatible, ethanol (C_2H_5OH A.R.) is acted as a solvent. BP was purchased from XF NANO Inc. (NanJing, China). Hydrochloric acid (HCl A.R.) is utilized as the catalyst.
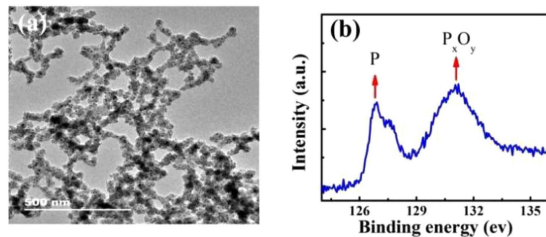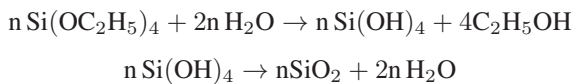

Fig. 2.   Characterization of BP: (a) Representative low-resolution TEM (scale bars, 500 nm). (b) XPS spectra. The peak at 131.2 eV is generated by P_xO_y, implying that BP has been partial oxidized.

powder is dispersed into 10-ml alcohol and the mixture is treated under sonication condition for three hours to obtain BP solution. Then, TEOS, alcohol, BP solution and water are been mixed up with each other, and the molar ratio of H_2O: C_2H_5OH: TEOS is 4:10:1. Because water and TEOS are incompatible, C_2H_5OH is acted as a solvent. The mixture is stirred for three hours to make water contact with TEOS. Next, 0.05-ml hydrochloric acid is added to promote this reaction. The mixed solution is aged for two days to form a sol. Finally, the sol is poured into a box, and left to age at room temperature to form BP-doped solid glass. The mass fraction of BP is 0.97%. The reaction equation is described as follows:

$$n\,Si(OC_2H_5)_4 + 2n\,H_2O \rightarrow n\,Si(OH)_4 + 4C_2H_5OH$$

$$n\,Si(OH)_4 \rightarrow nSiO_2 + 2n\,H_2O$$

B. Characterization of the BP

The morphology features of BP are investigated using a transmission electron microscopy (TEM, JEM-2100), as shown in Fig. 2(a). In order to explore the stability of BP in the air, BP is exposed to air for five days before measuring. Then, the element composition and chemical structure of BP are studied by X-ray photoelectron spectroscopy (XPS, AXIS ULTRA). The peak of 131.2 eV is generated by the P_xO_y, so it is important to stabilize BP in the air- see Fig. 2(b).
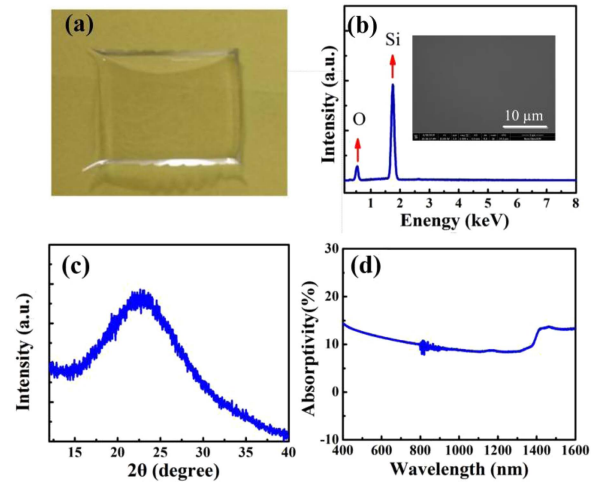

Fig. 3.   Characterization of sol-gel glass: (a) Digital photos. The surface topography is smooth and compact. (b) EDS spectrum. The main elements of the sol-gel glass are O and Si. (c) X-ray diffraction spectrum. It is the peak of amorphous silicon dioxide. (d) Linear absorptivity spectra. The absorptivity of sol-gel glass is measured in the range form 400 nm to 1600 nm, the transmittance is 14% at the wavelength of 1530 nm.

C. Characterization of Pure Sol-Gel Glass

The pure sol-gel glass is a colorless transparent sheet as shown in Fig. 3(a). The surface character of the sol-gel glass is studied by Scanning Electron Microscope (SEM, Nova Nano SEM Training-X50 series), the surface topography is smooth and compact - see the illustration in Fig. 3(b). The main elements of the sol-gel glass are O and Si, which are investigated by annex-energy spectrometry (EDS). Finally, X-ray diffraction (XRD) testifies that the main component of the sample is amorphous silicon dioxide as shown in Fig. 3(c). Fig. 3(d) shows that the absorptivity of pure sol-gel glass is very low, ranging from 5% to 15%, indicating it is a promising host material for SA.

D. Characterization of BP-Doped Sol-Gel Glass

The BP-doped sol-gel glass composites are exposed to air for five months before detection. As shown in Fig. 4(a), the typical BP-doped sol-gel glass is grey and transparent, indicating that BP is uniformly dispersed to sol-gel glass. The EDS is used to verify the compositional elements of BP-doped sol-gel glass, as shown in the figure, the main component elements of the sample are O, Si, and P-see Fig. 4(b). Because the XPS can only detect the surface composition of the sample, the spectra shows that the contents of O, Si, C are only included, without the peak of BP, indicating the BP is successfully encapsulated in the sol-gel glass (Fig. 4(c)). The Raman spectra (LabRam confocal Microprobe Raman system) is used to characterize the structures of BP-doped sol-gel glass. As shown in the Fig. 4(d), three main absorption peaks centered at 360, 437, 465 cm^{-1} can be clearly seen. The peak at 360 cm^{-1} is associated with vibration mode A_{1g}, the peaks at 437 cm^{-1} and 465 cm^{-1} arouse from two in-plane vibration modes B_{2g} and A_{2g}. It has been shown that the intensity ratio of the A_{g1}/A_{g2} phonon sensitively depends on sample degradation as a result of oxidation [7]. The intensity
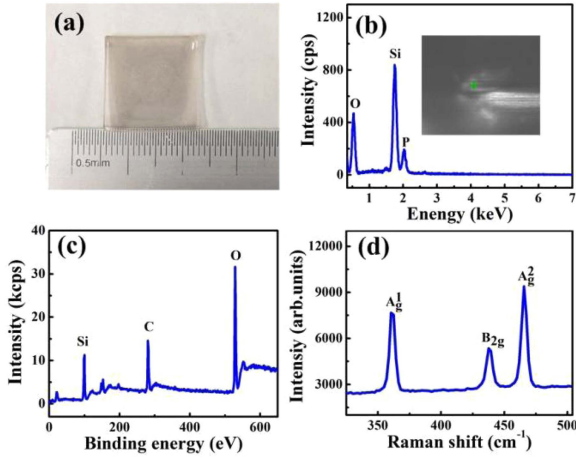
Fig. 4. Characterization of BP-doped sol-gel glass: (a) Digital photos. The typical BP-doped sol-gel glass is grey. (b) EDS spectrum. The component elements of the sample are O, Si, P. (c) XPS spectra. The contents of O, Si, C are only included, without the peak of P. (d) Typical Raman spectra of BP.
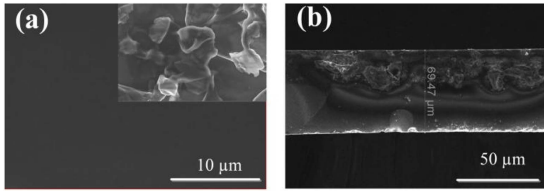

Fig. 5. Characterization of BP-doped sol-gel glass: (a) SEM image; (b) side profile image.

ratio of A_{1g}/A_{2g} is 0.9, indicating there is no oxidation of the BP nanosheets.

The morphology features of BP-doped sol-gel glass are investigated using a SEM. Because the BP is encapsulated by sol-gel glass, the SEM diagram of the Fig. 5(a) shows that the surface of the BP-doped sol-gel glass is smooth and compact, without the features of BP. The illustration shows the layered structure of pure BP. As shown in illustration of Fig. 5(b), the thickness of the BP-doped sol-gel glass is measured as 69.47 μm by SEM. When used, the BP-doped sol-gel glass is cut to 1 mm × 1 mm pieces and sandwiched between two fiber connectors.

III. APPLICATION FOR PULSE GENERATION

A. Optical Properties of BP-Doped Sol-Gel Glass

In an attempt to explore the stability of BP-doped sol-gel glass in the air, it is exposed to air for five months before measuring. The nonlinear saturable absorption property of the BP-doped sol-gel glass is investigated by a balanced twin-detector measurement technique, as shown in Fig. 6(a). A home-made ultrafast laser (central wavelength: 1560 nm, pulse duration: 500 fs, repetition rate: 26.43 MHz) is used as the light source. According to the fitting analysis, the modulation depth and saturable influence are estimated to be 1.4%, 7.8 MW/cm^2 respectively (Fig. 6(b)).

The pulsed laser-induced optical damage thresholds of BP/PMMA film, and BP-doped sol-gel glass are measured by a femtosecond Ti: sapphire laser at central wavelength of
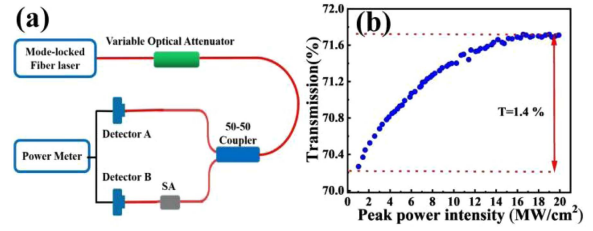

Fig. 6. (a) Balanced twin-detector optical absorption measurement setup. (b) Power-dependent transmission.
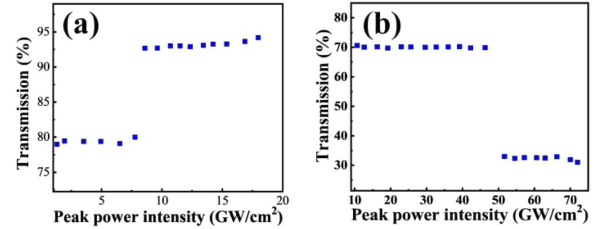

Fig. 7. (a) Damage-threshold measurement for BP/PMMA; (b) damage-threshold measurement for BP-doped sol-gel glass.
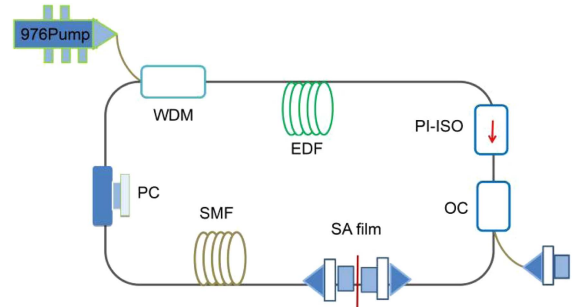

Fig. 8. Experimental setup for the Q-switching laser. WDM, wavelength division multiplexer; EDF, erbium-doped fiber; PI-ISO, polarization independent isolator; OC, output coupler; SA, saturable absorber; SMF, sing-mode fiber; PC, a polarization controller.

1030 nm, pulse duration of 250 fs, and repetition rate of 100 kHz. When the input peak power is below 8.59 GW/cm^2, transmittance of BP/PMMA film has been maintained at 78.6% and there is no damage. The BP/PMMA will be burnt out by the higher peak power, linear transmission of BP/PMMA roses to nearly 100% as shown in Fig. 7(a), which implies that damage threshold of BP/PMMA is 8.59 GW/cm^2. For BP-doped sol-gel glass, it begins to crack when input peak power exceeds 51.69 GW/cm^2. Due to the diffuse reflection of laser, the transmittance begins to decrease. The damage threshold of BP-doped sol-gel glass is estimated as 51.69 GW/cm^2 -see Fig. 7(b).

B. Setup of Fiber Laser

The schematic diagram of the fiber laser is schematically depicted in Fig. 8. The all-fiber laser oscillator consists of a 980/1550 nm wavelength division multiplexer (WDM), a 3-m EDF, a polarization independent isolator (PI-ISO), a polarization controller (PC), a BP-doped sol-gel glass stored for five months in the air, and a 40% output coupler (OC). A 976-nm laser
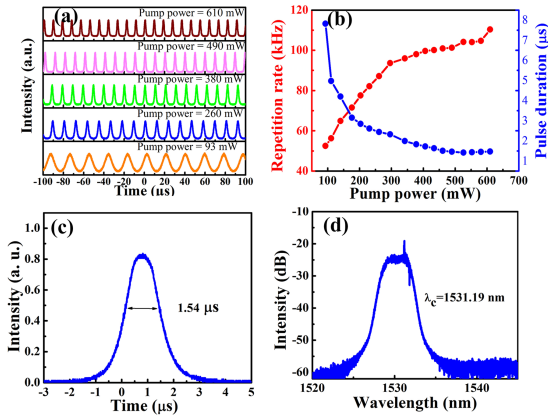
Fig. 9. Typical characteristics of Q-switching pulses: (a) Pulse trains under the pump power of 93 mW, 260 mW, 380 mW, 490 mW, and 610 mW. (b) Pulse repetition frequency and pulse duration as a function of pump power. Red shading shows pulse repetition frequency, blue shading shows pulse duration. (c) Single pulse profile. (d) The emission spectrum.

diode is used as the pump source. The EDF with an absorption coefficient of 25 dB/m at 1530 nm is utilized as the gain medium. A PI-ISO is placed inside the laser cavity to ensure unidirectional operation. In order to optimize the polarization state of the circulating laser, a PC is used to select different optical modes. The BP-doped sol-gel glass is sandwiched between two fiber connectors. The tail fibers of all devices are standard sing-mode fiber (SMF). 40% of laser is employed as output by OC, which is detected using an optical spectrum analyzer (JDSUOLP-85), a 1-GHz digital oscilloscope (Rohde & Schwarz, RTO1014) with a home-made 5-GHz photodiode detector, and a radio- frequency analyzer (Rohde & Schwarz FSV 13).

C. Experimental Results and Analysis

When the input pump power reaches 56 mW, the EDF laser starts to output the continuous wave. The stable Q-switching pulse trains are first obtained at the pump power of 93 mW, and can be kept until the pumping power up to 610 mW. Fig. 9(a) shows five typical pulse trains at different pump powers of 93 mW, 260 mW, 380 mW, 490 mW and 610 mW, respectively. By increasing the laser pump power, the repetition frequency goes from 52.48 kHz to 110.32 kHz, and the pulse width of Q-switching is narrowed, as shown in Fig. 9(b). A smooth and symmetric single pulse envelope is shown in Fig. 9(c), which shows a pulse duration of 1.54 μs. There is no obvious jitter in pulse shape, indicating that the Q-switched operation is stable. Fig. 9(d) shows the corresponding optical spectrum, which illustrates the spectra centred at 1531.19 nm.

Fig. 10 shows the average output power as a function of the pump power. The maximum average output power is obtained to be 34.86 mW at the pump power of 610 mW, while the maximum single pulse energy is 315.99 nJ. Therefore, BP-doped sol-gel glass can endure an incident power of 610 mW, indicating BP is effectively protected by sol-gel glass.

In order to obtain mode-locked operation, we replace a different SA, the optical setup has not changed. Because the saturable absorption of BP varies depending on its concentration, and the distribution of BP concentration in sol-gel glass
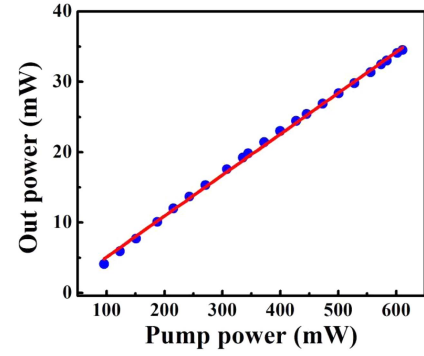

Fig. 10. Relationship between pump power and output power: The output power increases linearly with pump power.
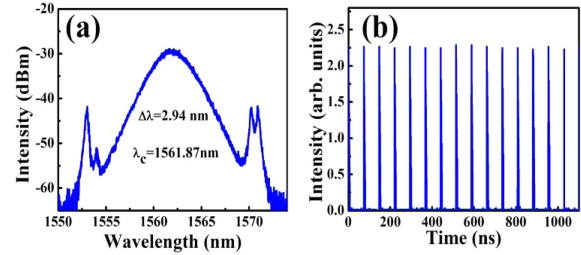

Fig. 11. (a) Measured the optical spectrum. (b) Pulse trains of oscilloscope.

TABLE I
TYPICAL Q-SWITCHED FIBER LASERS BASED ON 2D MATERIAL

SA type	Pump power (mW)	T (μs)	E (nJ)	Out power (mW)	Ref
Graphene	6.5-82.8	3.7	16.7	1.1	31
TiS$_2$	20-39	4	9.5	-	32
Antimonene	41-345	21.58	37.9	2.85	33
PbS/CdS	80-120	3.3	142	6	34
Bi$_2$Se$_3$	136–195	8.46	0.65	0.038	35
BP	50-195	10.32	94.3	1.5	36
BP	23-55	3.16	16.8	0.728	37
ZrS$_2$	144-479	2.3	53.0	4.08	38
TaSe$_2$-PVA	41-515	1.53	65.5	2.98	19
Bi$_2$Se$_3$- PVA	96-360	1.9	23.8	22.35	20
InSe -PVA	190-412	8.3	112.97	1.425	21
Al$_2$O$_3$-PVA	158-330	2.8	56.7	4.5	22
PtS$_2$ -PVA	53-84	4.2	45.6	1.1	23
Cr$_2$AlC- PVA	117 -167	0.780	9	1.134	24
BP- PVA	32 -231	3.59	142.60	4.2	25
BP-SiO$_2$	93-610	1.53	315.99	34.86	Our

is could be controlled. A piece of BP-doped sol-gel glass with a higher concentration is applied to the same laser cavity as a SA. The content of BP in BP-doped sol-gel glass is 1.46%. By properly adjusting the PC, a mode-locked pulse is achieved as shown in Fig. 11. The output spectrum has a pair of symmetric sideband (Fig. 11(a)), which implies it is a typical conventional soliton. It is centered at 1561.87 nm with a 3-dB spectral bandwidth of 2.94 nm. As shown in Fig. 11(b), the pulse interval is estimated to be 73.42 ns, which is agreed with the cavity length.

When BP-doped sol-gel glass is replaced with sol-gel glass in the laser cavity, no pulses are generated, which suggests that the saturable absorption properties of the BP play crucial roles in starting and stabilizing the laser pulses. These results prove that BP-doped sol-gel glass can also be used as a mode-locked device, and the potential for further applications in fiber laser.

The previous Q-switched EDF lasers with 2D material as SAs are presented in Table I. The output power and the single pulse energy of our work are relatively high at the 1.5 μm region. In addition, the Q-switching fiber laser works in a wide pump range, owing to the prepared high quality BP-doped sol-gel glass with high optical damage threshold. These results prove that BP-doped sol-gel glass has great potential advantages in the application of high power lasers.

IV. CONCLUSION

In conclusion, the air-stable BP film with high damage threshold is successfully prepared by means of low-temperature sol-gel technique. The main component of sol-gel glass is proved to be compact amorphous silicon dioxide by SEM, EDS, and XRD. By using a BP-doped sol-gel glass maintained after five months in ambient storage, both Q-switched and mode locked operation are obtained in an EDF laser. Especially, the Q-switched laser demonstrates a maximum pulse energy of 315.99 nJ, tunable repetition rate from 52.48 kHz to 110.32 kHz, and a pulse width from 7.83 μs to 1.53 μs. These results clearly show the performance of BP-doped sol-gel glass as an excellent SA, and the potential for further applications in high power fiber laser.

REFERENCES

[1] X. Wang et al., "Highly anisotropic and robust excitons in monolayer black phosphorus," *Nature Nanotechnol.*, vol. 10, no. 6, pp. 517–521, Jun. 2015.

[2] L. Li et al., "Black phosphorus field-effect transistors," *Nature Nanotechnol.*, vol. 9, no. 5, pp. 372–377, May 2014.

[3] J. Qiao, X. Kong, Z. X. Hu, F. Yang, and W. Ji, "Few-layer black phosphorus: Emerging 2D semiconductor with high anisotropic carrier mobility and linear dichroism," *Nature Commun.*, vol. 5, 2014, Art. no. 4475.

[4] W. C. Huang et al., "Emerging black phosphorus analogue nanomaterials for high-performance device applications," *J. Mater. Chem. C*, vol. 8, no. 4, pp. 1172–1197, Jan. 2020.

[5] B. Zhang et al., "Exfoliated layers of black phosphorus as saturable absorber for ultrafast solid-state laser," *Opt. Lett.*, vol. 40, no. 16, pp. 3691–3694, Aug. 2015.

[6] J. Sotor, G. Sobon, M. Kowalczyk, W. Macherzynski, P. Paletko, and K. M. Abramski, "Ultrafast thulium-doped fiber laser mode locked with black phosphorus," *Opt. Lett.*, vol. 40, no. 16, pp. 3885–3888, Aug. 2015.

[7] D. Hanlon et al., "Liquid exfoliation of solvent-stabilised black phosphorus: Applications beyond electronics," *Nature Commun.*, vol. 6, pp. 8563–8573, Oct. 2015.

[8] S. B. Lu et al., "Broadband nonlinear optical response inmulti-layer black phosphorus: An emerging infrared and mid-infrared optical material," *Opt. Exp.*, vol. 23, no. 9, pp. 11183–11194, Apr. 2015.

[9] M. Zhang et al., "2D Black phosphorus saturable absorbers for ultrafast photonics," *Adv. Opt. Mater.*, vol. 7, no. 1, Jan. 2019, Art. no. 1800224.

[10] G. G. Andres et al., "Isolation and characterization of few-layer black phosphorus," *2D Mater.*, vol. 1, no. 2, Jun. 2014, Art. no. 025001.

[11] M. Wang et al., "Functional two-dimensional black phosphorus nanostructures 2 towards next-generation devices," *J. Mater. Chem. A*, vol. 9, pp. 12433–12473, Apr. 2021.

[12] N. R. Mishra, R. K. Nirala, R. P. Pandey, R. P. Ojha, and R. Prakash, "Homogenous dispersion of MoS$_2$ nanosheets in polyindole matrix at air–Water interface assisted by langmuir technique," *Langmuir*, vol. 33, no. 47, pp. 13572–13580, 2017.

[13] G. Liu et al., "Single- and dual-wavelength passively mode-locked erbium-doped fiber laser based on antimonene saturable absorber," *IEEE Photon. J.*, vol. 11, no. 3, Jun. 2019, Art. no. 1503011.

[14] Y. Chen et al., "Large energy, wavelength widely tunable, topological insulator Q-switched erbium-doped fiber laser," *IEEE J. Sel. Topics Quantum Electron.*, vol. 20, no. 5, Sep./Oct. 2014, Art. no. 0900508.

[15] J. D. Wood, S. A. Wells, D. Jariwala, and K. S. Chen, "Effective passivation of exfoliated black phosphorus transistors against ambient degradation," *Nano Lett.*, vol. 14, no. 12, pp. 6964–6970, Oct. 2014.

[16] H. Liu, X. C. Cheng, and Q. Fen, "A new strategy for air-stable black phosphorus reinforced PVA nanocomposites," *J. Mater. Chem. A*, vol. 6, no. 16, pp. 7142–7147, Jan. 2018.

[17] Z. Liu, B. Zhang, N. Dong, J. Wang, and Y. Chen, "Perfluorinated gallium phthalocyanine axially grafted black phosphorus nanosheets for optical limiting," *J. Mater. Chem. C*, vol. 8, pp. 10197–10203, 2020.

[18] X. Zhu et al., "Stabilizing black phosphorus nanosheets via edge-selective bonding of sacrificial C$_{60}$ molecules," *Nature Commun.*, vol. 9, 2018, Art. no. 4177.

[19] X. Liu, Z. Hong, Y. Liu, H. Zhang, and X. Ge, "Few-layer TaSe$_2$ as a saturable absorber for passively Q-switched erbium-doped fiber laser," *Opt. Mater. Exp.*, vol. 11, no. 2, pp. 385–397, 2021.

[20] Z. Yu et al., "High-repetition-rate Q-switched fiber laser with high quality topological insulator Bi$_2$Se$_3$ film," *Opt. Exp.*, vol. 22, no. 10, pp. 11508–11515, 2014.

[21] W. Yang, N. Xu, and H. Zhang, "Nonlinear absorption properties of indium selenide and its application for demonstrating pulsed Er-doped fiber laser," *Laser Phys. Lett.*, vol. 15, no. 10, 2018, Art. no. 105101.

[22] S. K. M. Al-Hayali, D. Z. Mohammed, W. A. Khaleel, and A. H. Al-Janabi, "Aluminum oxide nanoparticles as saturable absorber for C-band passively Q-switched fiber laser," *Appl. Opt.*, vol. 56, no. 16, pp. 4720–4726, 2017.

[23] X. Wang et al., "Laser Q-switching with PtS$_2$ microflakes saturable absorber," *Opt. Exp.*, vol. 26, no. 10, pp. 13055–13060, 2018.

[24] M. M. Najm et al., "Chromium aluminum carbide as Q-switcher for the near-infrared erbium-doped fiber laser," *Optik*, vol. 250, Nov. 2022, Art. no. 168362.

[25] H. Mu et al., "Black phosphorus-polymer composites for pulsed lasers," *Adv. Opt. Mater.*, vol. 3, no. 10, pp. 1447–1453, Oct. 2015.

[26] H. Zhang, Q. Bao, D. Tang, L. Zhao, and K. Loh, "Large energy soliton erbium-doped fiber laser with a graphene-polymer composite mode locker," *Appl. Phys. Lett.*, vol. 95, no. 14, Oct. 2009, Art. no. 141103.

[27] N. M. Yusoff, E. K. Ng, N. S. Rosli, C. A. C. Abdullah, N. M. Yusoff, and M. A. Mahdi, "TiO$_2$-SiO$_2$ nanocomposite saturable absorber for ultrafast photonics," *IEEE Photon. J.*, vol. 15, no. 1, Feb. 2023, Art. no. 1500610.

[28] Z. D. Chen, H. Y. Wang, Y. G. Wang, R. D. Lv, X. G. Yang, and J. Wang, "Improved optical damage threshold graphene Oxide/SiO$_2$ absorber fabricated by sol-gel technique for mode-locked erbium-doped fiber lasers," *Carbon*, vol. 144, pp. 737–744, Dec. 2019.

[29] R. F. S. Lenza and W. L.Vasconcelos, "Preparation of silica by sol-gel method using formamide," *Mater. Res.*, vol. 4, no. 3, pp. 189–194, 2001.

[30] X. T. Ma, J. L. Liu, C. Zheng, W. L. Huang, S. G. Cai, and X. Q. Xiao, "Passivation of black phosphorus nanoflakes embedded in a silica glass matrix affords ambient saturable absorption stability enhancement," *Appl. Opt.*, vol. 61, no. 15, May 2022, Art. no. 4638.

[31] Z. Luo et al., "Graphene-based passively Q-switched dual-wavelength erbium-doped fiber laser," *Opt. Lett.*, vol. 35, no. 21, pp. 3709–3711, Nov. 2010.

[32] X. Zhu et al., "TiS$_2$-based saturable absorber for ultrafast fiber lasers," *Photon. Res.*, vol. 6, no. 10, pp. C44–C48, Oct. 2018.

[33] P. Hu et al., "Passively Q-switched erbium-doped fiber laser based on antimonene as saturable absorber," *Appl. Opt.*, vol. 58, no. 28, pp. 7845–7850, Oct. 2019.

[34] S. Yang, F. Li, M. M. Gong, L. Zhang, Z. W. Zhu, and H. B. Shen, "Generation of Q-switched and mode-locked pulses based on PbS/CdS saturable absorbers in an Er-doped fiber laser," *J. Mater. Chem. C*, vol. 15, no. 10, pp. 5956–5961, May 2022.

[35] S. R. Azzuhri, H. Ahmad, A. M. A. M. Salim, M. R. K. Soltanian, and S. W. Harun, "Passively dual-wavelength Q-switched ytterbium doped fiber laser using selenium bismuth as saturable absorber," *J. Modern Opt.*, vol. 62, no. 19, pp. 1550–1554, Jun. 2015.

[36] Y. Chen et al., "Mechanically exfoliated black phosphorus as a new saturable absorber for both Q-switching and mode-locking laser operation," *Opt. Exp.*, vol. 23, no. 10, pp. 12823–12833, May 2015.

[37] D. Li et al., "Polarization and thickness dependent absorption properties of black phosphorus: New saturable absorber for ultrafast pulse generation," *Sci. Rep.*, vol. 5, 2015, Art. no. 15899.

[38] L. Li et al., "Optical nonlinearity of ZrS$_2$ and applications in fiber laser," *Nanomaterials*, vol. 9, no. 3, pp. 315–321, Feb. 2019.